HIGH-SPEED COMPUTATION AND EXPERIMENT ON ADDED-MASS AND VISCOUS-DAMPING FORCES ACTING ON VARIOUS OSCILLATING 3D OBJECTS

Ryuta Tanaka[+1], Hajime Onishi[+1], Hideki Shimohara[+2],
Hirochika Tanigawa[+3] and Katsuya Hirata[+1]

[+1] Department of Mechanical Engineering Doshisha University, Kyoto, Japan
[+2] Doshisha International High School, Kyoto, Japan
[+3] Department of Mechanical Engineering, NIT, Maizuru College, Kyoto, Japan

In many fluid-structure-interaction problems, the added mass is one of important interests. In the present study, we propose a simple and efficient method to specify fluid-force coefficients of a three-dimensional oscillating object in viscous fluid. The solving method is based on a discrete singularity method DSM. Then, we apply the DSM to some three-dimensional basic objects such as square-cross-section cylinders with various aspect ratios. Furthermore, we conduct experiments, and reveal the fluid-force coefficients of them comparing between computations and experiments, which show good agreement.

Keyword: Fluid Force, Numerical Analysis, Added Mass, Virtual Mass,
          Discrete Singularity Method

1. INTRODUCTION

In many fluid-structure interaction problems, we often needed to consider the fluid forces caused by arbitral accelerated motions of fluid and/or solid objects. Such forces have been understood using the concept of "the added mas," "the virtual mass," "the carried mass" or "included mass." Then, the added mass is one of important and essential interests in various engineering aspects such as marine vehicles and structures. In general, we need to consider the added mass of the fluid in arbitral accelerated motion. One of the simplest and the most fundamental accelerated motion is a periodical-forcing case, that is, (1) a sinusoidally-oscillating solid object in stationary fluid and (2) a stationary solid object in sinusoidally-moving fluid. Both the cases (1) and (2) are identical under the assumption of infinitesimal amplitudes, as one can be approximatelly converted into the other by considering the Floude-Krylov force.[1] & [2] So, we now consider the case (1). Due to the importance of the added mass, there have been many past studies in concern, which are mainly related with two-dimensional flow.[3] - [13] However, there have been a few researches concerning the three-dimensional flow around a three-dimensional object,[16] - [21] despite its importance in various industrial aspects.

In the present study, we propose a simple method where the solving method is based on a discrete singularity method (hereinafter, referred to as DSM) in order to specify the added mass of a three-dimensional object, as well as our previous studies[14] & [15] for a two-dimensional object. In this method, we consider an incompressible viscous fluid under the assumption of an infinitesimal oscillation amplitude of an object, and properly modify the three-dimensional full Navier-Stokes equations, namely, into linear equations the Brinkman equations. In two-dimensional-flow problems, we can introduce complex-variable functions supposing the Gauss-Argand planes. Instead, in the present three-dimensional-flow problems, we employ a fundamental solution of the Brinkman equations proposed by Tsai[22] as a singularity of the DSM. Furthermore, we conduct experiments, and attempt to reveal the fluid-force coefficients of them comparing between computations and experiments.

[+1]khirata@mail4.doshisha.ac.jp, [+3]tanigawa@maizuru-ct.ac.jp

2. MODEL, GOVERNING PARAMETERS AND FLUID FORCE
(1) Model

Figure 1 shows the concept of model. A three-dimensional object sinusoidally oscillates in stationary and infinite fluid with incompressibility and viscosity. The object's displacement is given by $x = A\sin(\omega t)$, $y = 0$ and $z = 0$, where t denotes time.

(2) Governing parameters

Dimensionless governing parameters are kinetic Reynolds number S ($\equiv \omega L^2/v$) and Keulegan-Carpenter number KC ($\equiv 2\pi A/L$), where L and v denote a characteristic length scale and the viscosity of fluid, respectively. In the present study, we discuss various square-cross-section cylinders with low aspect ratios as the oscillating object. Figure 2 is those models. The cylinders with an aspect ratio b/a oscillates in the x direction, where a and b denote a side length and a height of the cylinder, respectively. V is the volume of the cylinder, and L is an equivalent diameter d_e ($\equiv (6V/\pi)^{1/3} = (6a^2b/\pi)^{1/3}$). We consider both the cylinder in transverse oscillation like figure(a) and the cylinder in axial oscillation like figure(b). Tables 1 and 2 summarise the range of the governing parameters in computation and experiment, respectively.

(3) Fluid force

We solely consider the three-dimensional object whose cross section is symmetric on an arbitrary plane parallel to the x-axis. Then, the flow can be symmetric to the x-axis on every planes parallel to the x-axis, as well. In such a case, as the y- and z-components F_y and F_z of the fluid force $\boldsymbol{F}$ acting on the object is cancelled out into zero, the x-component F_x is exclusively meaningful. Following to Chen,[6] we normalise F_x as a non-dimensional fluid force H_x. The real part $\mathrm{Re}(H_x)$ and the imaginary part $\mathrm{Im}(H_x)$ of H_x denote an added-mass coefficient and a negative damping coefficient, respectively. Then, we refer to $-\mathrm{Im}(H_x)$ as a damping coefficient. —In some cases, we conventionally use the drag and inertia coefficients C_D and C_M as alternates to $\mathrm{Re}(H_x)$ and $-\mathrm{Im}(H_x)$. The definitions of C_D and C_M are given by the Morison's equation.[28]—

3. NUMERICAL PROCEDURE
(1) Linear approximation

The governing equations for incompressible and viscous flow are the three-dimensional Navier-Stokes equations and the continuity equation. We linearly approximate them under the assumption of an infinitesimal amplitude, and get the Brinkman equations and continuity equation as the present governing equations.[14) & 15)]

(2) DSM

Now, we consider a DSM[5), 14), 15), 24) - 27)] to solve the linearly-approximated governing equations, numerically. A fundamental solution of the governing equations; namely, a three-dimensional Brinkmanlet is given by Tsai (2008).[22] Figure 3 shows an analytical model of the DSM for a square cross-section cylinder, where singularities and control points are arranged inside and on the cylinder, respectively.

4. EXPERIMENTAL PROCEDURE
(1) Theory

We consider the Newton's second law of motion of a pendulum in fluid. In the small angle approximation,[29] we get the coordinate s measured along the arc of the pendulum in damping free oscillation as follows.

$$s(t) = A e^{-\zeta \omega_n t}\sin(\omega_n t) \qquad \text{with} \qquad \omega_n = \sqrt{\frac{m_g}{m_i}}\,\omega_a \quad \text{and} \quad \zeta = \frac{C}{2\omega_a\sqrt{m_g m_i}} \quad , \qquad (1)$$

where C denotes the damping factor. The mass corresponding to the gravitational force is m_g, and the mass

reacting to acceleration is m_i for the pendulum. ω_n denotes the natural frequency (angular frequency at $C = 0$), and ζ denotes the damping ratio. ω_a $(\equiv \sqrt{g/l})$ is the natural frequency in a, which is taken to be equivalent to that in vacuum. We should note that $\sqrt{1 - \zeta^2} = 0.999 - 1.000 \approx 1$ as for the present experiments. Then, $\text{Re}(H_x)$ and $-\text{Im}(H_x)$ are given by the following equations.

$$\text{Re}(H_x) \left(= C_M\right) = \left(\frac{\omega_a}{\omega_n}\right)^2 \left(\frac{\rho_o}{\rho} - 1\right) - \frac{\rho_o}{\rho} \quad \text{and} \quad -\text{Im}(H_x) = \frac{2\zeta\omega_n}{\omega_n} \left(\frac{\rho_o}{\rho} + C_M\right) , \quad (2)$$

where ρ and ρ_o are the densities of fluid and the object, respectively. Both ω_n and $\zeta\omega_n$ are obtained from the time history of the object's motion in damping free oscillation.

(2) Experimental apparatus

Figure 4 shows the schematic diagram of the present experimental apparatus. Figure(a) represents an overall view. We fill a tank made from acrylics with water. And, a pendulum in water is hung above the tank by a knife edge. A high-speed video camera is perpendicularly installed to the oscillating plane of the pendulum. The recorded motion of the pendulum is analysed using a picture-correlation method. And, we can observe the time history of the object's motion in damping free oscillation. Figure(b) shows the dimensions of the pendulum and the tank. Figure(c) shows the details of the pendulum.

5. RESULTS AND DISCUSSION

(1) Linear theory

Figure 5 summarises the computational results for the cylinders with $b/a = 0.5-5.0$ in transverse oscillation, in a range of $S = 10-10,000$. That is to say, this figure shows $\text{Re}(H_x)$ and $-\text{Im}(H_x)$ as functions of S in figures(a) and (b), respectively. An arrow in figure(a) is the experiment for the cylinder at $S \gg 1$ with $b/a = 1.0$ (cube).[11] A dashed line in each figure is the analytical solution for a sphere.[17]

We can see that $\text{Re}(H_x)$ and $-\text{Im}(H_x)$ have remarkable tendencies being independent of b/a. Namely, $\text{Re}(H_x)$ monotonically decreases and asymptotes to a certain value (potential theory), with increasing S. $-\text{Im}(H_x)$ monotonically decreases with increasing S, as well as $\text{Re}(H_x)$. In contrast with $\text{Re}(H_x)$, $-\text{Im}(H_x)$ asymptotes to zero at $S = \infty$. Of course, these tendencies of $\text{Re}(H_x)$ and $-\text{Im}(H_x)$ are the same as those for a sphere as shown in figure. The tendencies are appropriate, as the viscosity of fluid relatively decreases with increasing S.

Besides, we can discuss the effects of b/a upon $\text{Re}(H_x)$ and $-\text{Im}(H_x)$. Namely, both $\text{Re}(H_x)$ and $-\text{Im}(H_x)$ monotonically increase with increasing b/a. Both these b/a effects becomes less remarkable, when S increases. Thus, $-\text{Im}(H_x)$ becomes close to zero at $S > 10^3$ being independent of b/a. —From a quantitative point of view, both $\text{Re}(H_x)$ and $-\text{Im}(H_x)$ for a square cylinder with $b/a = 0.5$ are almost identical to those for a sphere at any S.— Both the b/a effects seem acceptable, because we regard the equivalent diameter as the present characteristic length scale. As for the b/a effect upon $\text{Re}(H_x)$, the projected area of a cylinder on the plane perpendicular to the direction of forced oscillation increases with increasing b/a. As for the b/a effect upon $-\text{Im}(H_x)$, the total surface area of a cylinder increases, when b/a increases from about unity.

As well as the cylinders in transverse oscillation, we get the computational results for the cylinders with $b/a = 0.5-5.0$ in axial oscillation. Again, we can see that $\text{Re}(H_x)$ and $-\text{Im}(H_x)$ have remarkable tendencies being independent of b/a. These tendencies are the same as those in transverse oscillation. In contrast, the effects of b/a upon $\text{Re}(H_x)$ and $-\text{Im}(H_x)$ are different from those in transverse oscillation. Namely, $\text{Re}(H_x)$ monotonically decreases with increasing S. This b/a effect upon $\text{Re}(H_x)$ does not become less remarkable, when S increases. $-\text{Im}(H_x)$ almost coincides with one another, then $-\text{Im}(H_x)$ is approximately determined by only S being independent of b/a. The b/a effect upon $\text{Re}(H_x)$ seems acceptable. Because the projected area of a cylinder on the plane perpendicular to the direction of forced oscillation decreases with increasing b/a. As for the b/a effect upon $-\text{Im}(H_x)$, we need further study over wider ranges of parameters than the present study.

(2) Experiments

a) Non-linearity

In this sub-section, we consider the experiment for a square-cross-section cylinder at $S =$ 4,900 with b/a = 1.0 (cube) in transverse oscillation as an example, comparing with the linear theory at $KC = 0$ (computational solution).

Figures 6(a) and (b) show the experimental $Re(H_x)$ and $-Im(H_x)$ as functions of KC, respectively. In each figure, a dashed line denotes the linear theory for comparison. In the present study, we conduct the all experiments in condition of $\sin\theta \approx \theta$. —In a preliminary experiment, we have demonstrated that we can suppose translation motion, if the angle θ of a pendulum less than 5°.—

At first, we see figure(a) ($Re(H_x)$). When KC decreases from 13 to zero, $Re(H_x)$ tends to monotonically decrease and to approaches to a constant value. More specifically, this approaching manner seems complicated. Thus, we divide the range of KC into two: namely, a small-amplitude range at $KC \lesssim 2$ and a large-amplitude range at $KC \gtrsim 2$. In the small-amplitude range, the approaching manner can be exponential. So, we approximate the experimental results by an empirical formula such as $Re(H_x) = 0.76(1 + 0.07KC^{3.9})$ using the least squares method, whose curve is drawn by a solid line in the figure. According to this empirical formula, we see that the approaching constant value at $KC = 0$ is 0.76, which almost coincides with the linear theory (0.73).

Second, we see figure(b) ($-Im(H_x)$). When KC decreases from 13 to zero, $-Im(H_x)$ as well as $Re(H_x)$ tends to monotonically decrease and to approaches to a constant value. More specifically, this approaching manner seems complicated. Thus, we divide the range of KC into two: namely, a small-amplitude range at $KC \lesssim 2$ and a large-amplitude range at $KC \gtrsim 2$. —We should note that these two ranges are the same as those of $Re(H_x)$. This fact suggests that the non-linearities in the two ranges are not qualitatively the same each other.— In the small-amplitude range, the approaching manner can be exponential, as well as $Re(H_x)$. So, we approximate the experimental results by an empirical formula such as $-Im(H_x) = 0.15(1 + 0.59KC^{1.6})$ using the least squares method, whose curve is drawn by a solid line in the figure. According to this empirical formula, we see that the approaching constant value at $KC = 0$ is 0.15, which almost coincides with the linear theory (0.13).

b) Comparison between linear theory and experiment

Figure 7 summarises the experiment for a square-cross-section cylinder in transverse oscillation at $KC = 0$, which are predicted on the basis of such empirical formula as Figure 6. Figure 7(a) and (b) show $Re(H_x)$ and $-Im(H_x)$ as functions of S, respectively. In each figure, solid lines denote the linear theory, and a dashed line denotes the linear theory for a sphere. We can confirm that $Re(H_x)$ by the experiment agree well with that by the linear theory at any S and b/a. As for the experiment in axial oscillation as well as that in transverse oscillation in Figure 7, we can again confirm that both $Re(H_x)$ and $-Im(H_x)$ by the experiment agree well with those by the linear theory at any S and b/a.

6. CONCLUSION

In order to specify the added mass of basic three-dimensional objects such as square-cross-section cylinders with various aspect ratios, we have solved linearly-modified three-dimensional Navier-Stokes equations considering an incompressible viscous fluid under the assumption of an infinitesimal oscillation amplitude of an object. Furthermore, we have conducted experiments, and revealed the fluid-force coefficients of the cylinders comparing between computations and experiments, which show good agreement.

7. ACKNOWLEDGEMENT

REFERENCES

1) Meneghini and Bearman: *Journal of Fluids and Structures*, Vol. 9, pp. 435−455, 1995.

2) Chakrabarti: *Handbook of Offshore Engineering*, Vol. 1, Elsevier, Amsterdam, pp. 158−160, 2005.

3) Patton: *ASME Paper*, No. 65-WA/UNT-2, pp. 1−7, 1965.

4) Dalton and Helfinstine: *Transactions of ASME*, Ser. D, Vol. 934, pp. 636−642, 1971.

5) Yano and Ooe: *Transactions of JSME, Ser. B*, Vol. 58, No. 554, pp. 3094−3099, 1992. (in Japanese)

6) Chen: Flow-Induced vibration of circular cylindrical structures, Hemisphere, New York, pp. 30−35, 1987.

7) Scolan and Faltinsen: *Journal of Fluids and Structures*, Vol. 8, pp. 201−230, 1994.

8) Zheng and Dalton: *Journal of Fluids and Structures*, Vol. 13, pp. 225−249, 1999.

9) Keulegan and Carpenter: Journal of Research of National Bureau of Standards, Vol. 60, No. 5, pp. 423−440, 1958.

10) Morison, et al.: *Petroleum Transactions of American Institute of Mining, Metallurgical, and Petroleum Engineers*, Vol. 189, pp. 149−157, 1950.

11) Sarpkaya: *Transactions of ASME, Ser. E*, Vol. 42, pp. 32−37, 1975.

12) Minamizawa and Endoh: *Kagaku Kogaku Ronbun-shu*, Vol. 9, No. 4, pp. 353−358, 1983. (in Japanese)

13) Bearman, et al.: *Applied Ocean Research*, Vol. 6, pp. 83−89, 1984.

14) Shimohara and Hirata: *Transactions of JSME, Ser. B*, Vol. 66, No. 644, pp. 1061−1066 , 2000. (in Japanese)

15) Shimohara, et al.: *Transactions of JSME, Ser. B*, Vol. 77, No. 782, pp. 1904−1919, 2011. (in Japanese)

16) Lamb, H.: *Hydrodynamics, 6th Ed.*, Dover Publications, New York, pp. 738, 1932.

17) Stokes: *Cambridge Philosophical Transactions*, Vol. IX, pt. 2, pp. 8−106, 1851.

18) Landau and Lifshitz: *2nd Ed.*, Pergamon Press, Oxford, pp. 89, 1987.

19) Isobe: *Applied Physics*, Vol. 17, No. 1−2 (a), pp. 250−253, 1948.

20) Isobe: *Applied Physics*, Vol. 17, No. 3−4 (b), pp. 55−59, 1948.

21) Inoue and Sato: *Bulletin of Japanese Society of Scientific Fisheries*, Vol. 51, No. 12, pp. 1997−2006, 1985. (in Japanese)

22) Tsai: International Journal for Numerical Methods in Fluids, Vol. 56, pp. 927−940, 2008.

23) Sarpkaya: *Journal of Fluids and Structures*, Vol. 21, pp. 435−440, 2005.

24) Yano, et al.: *Transactions of ASME, Journal of Applied Mechanics*, Vol. 63, pp. 990−996, 1996.

25) Tanigawa, et al.: *Transactions of JSME, Ser. B*, Vol. 66, No. 645, pp. 1300−1310, 2000. (in Japanese)

26) Tanigawa, et al.: *Transactions of JSME, Ser. B*, Vol. 69, No. 684, pp. 1854−1861, 2003. (in Japanese)

27) Hirata, et al.: *Transactions of JSME, Ser. B*, Vol. 74, No. 748, pp. 2485−2493, 2008. (in Japanese)

28) Morison, et al.: *Petroleum Transactions of American Institute of Mining, Metallurgical, and Petroleum Engineers*, Vol. 189, pp. 149−157, 1950.

29) Neill, et al.: *American Journal of Physics*, Vol. 75, pp. 226−229, 2007.
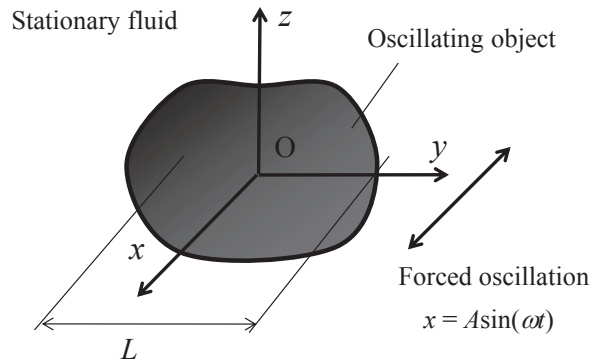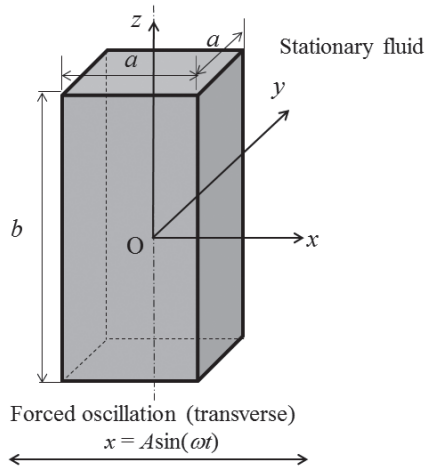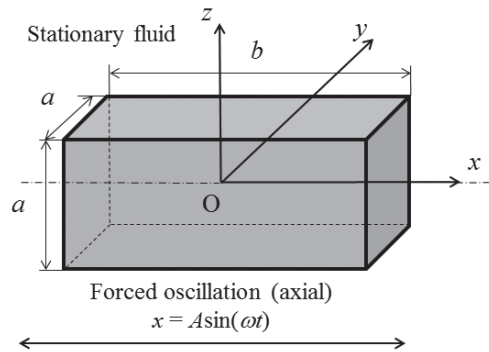
Figure 1: Model: an oscillating 3D object in stationary fluid.

(a) A cylinder oscillating perpendicularly to the cylinder's axis and
perpendicularly to a pair of opposing cylinder's lateral faces.

(b) A cylinder oscillating parallel to the cylinder's axis.

Figure 2: Model: an oscillating square-cross-section cylinder (right square prism)
with an aspect ratio b/a in stationary fluid.

Table 1: Parameters in linear analyses.

	b/a	S	KC
In transverse oscillation	0.5–5.0	10–10,000	0
In axial oscillation	0.5–5.0	10–10,000	0

Table 2: Parameters in experiments.

	b/a	S	KC
In transverse oscillation	1.0, 2.0, 3.0 and 4.0	1,600–7,300	0.065–13
In axial oscillation	1.0, 2.0 and 3.0	1,600–7,800	0.065–13

(a) Top view

(b) Front view of a cross section
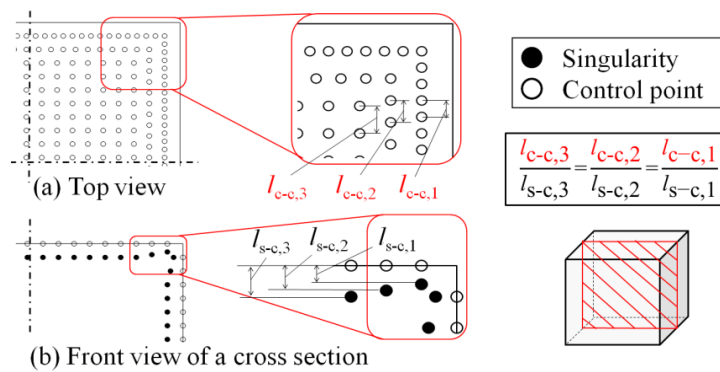
Figure 3: An analytical model of DSM for a corner of a square-cross-section cylinder.
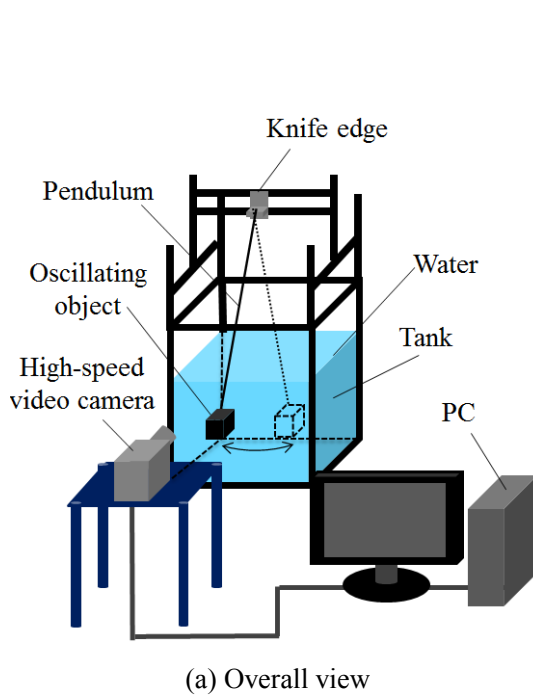
(a) Overall view

(b) Dimensions of a pendulum and a tank (unit: mm)

(c) Details of a pendulum
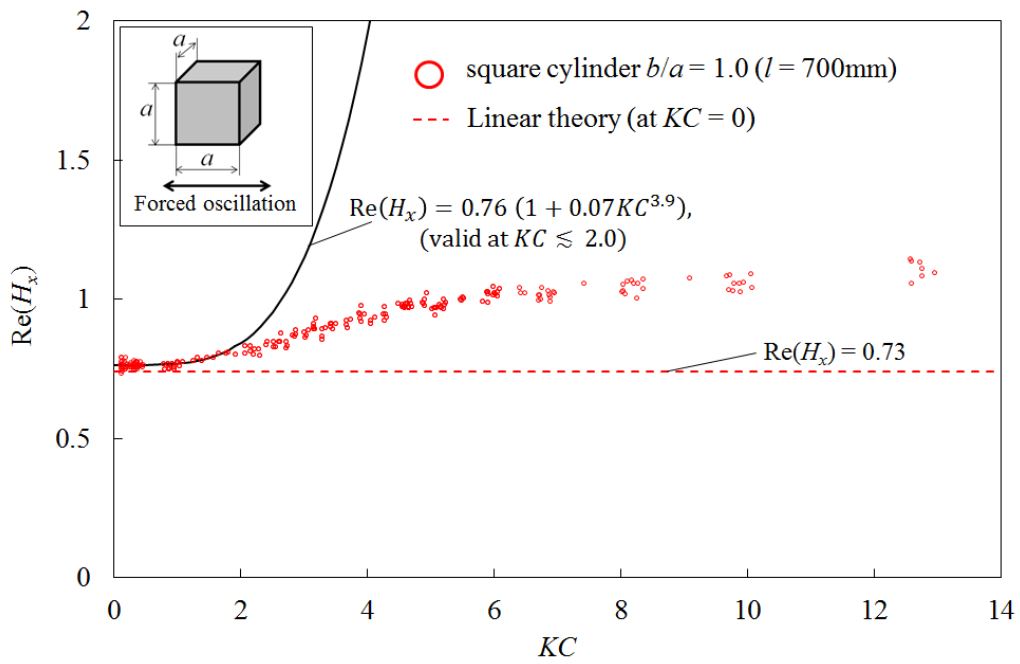
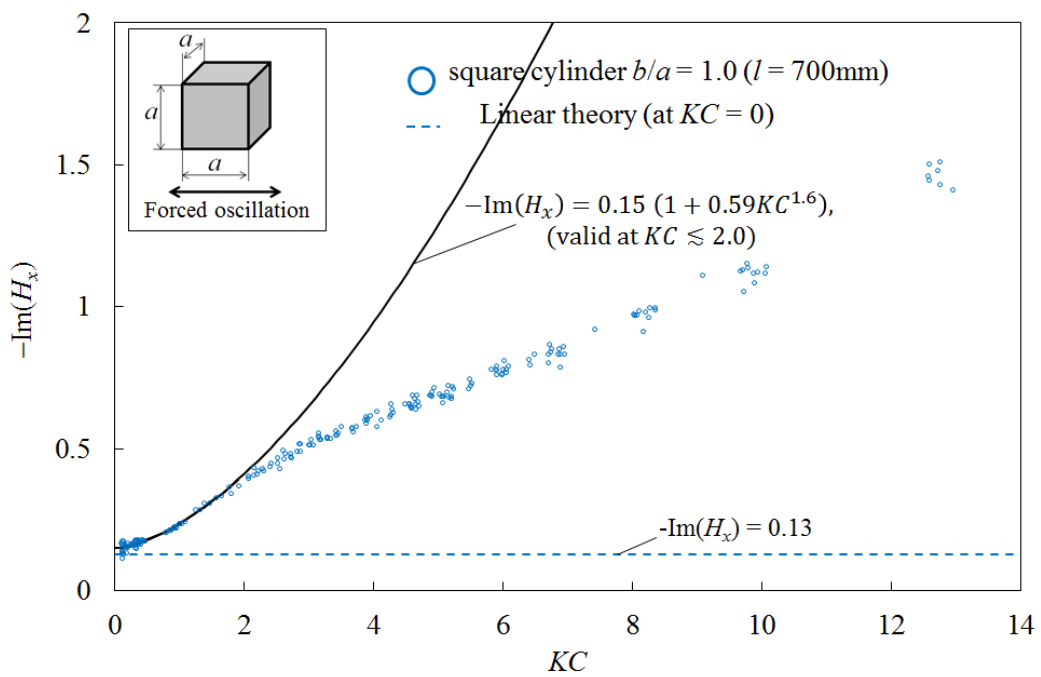Figure 4: Schematic diagram of experimental apparatus.
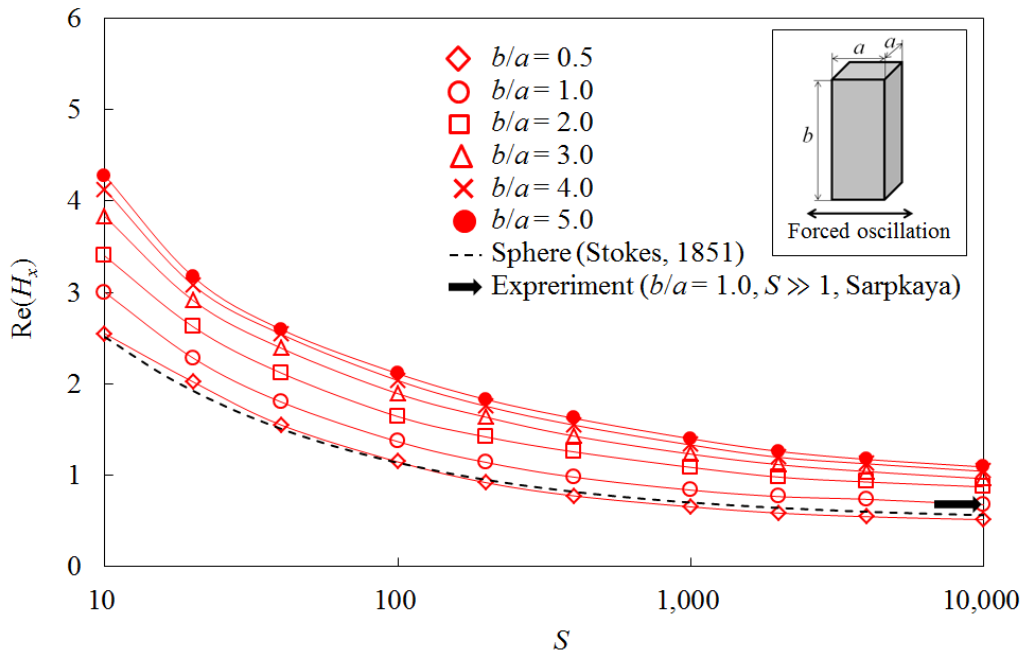
(a) Re(H_x)
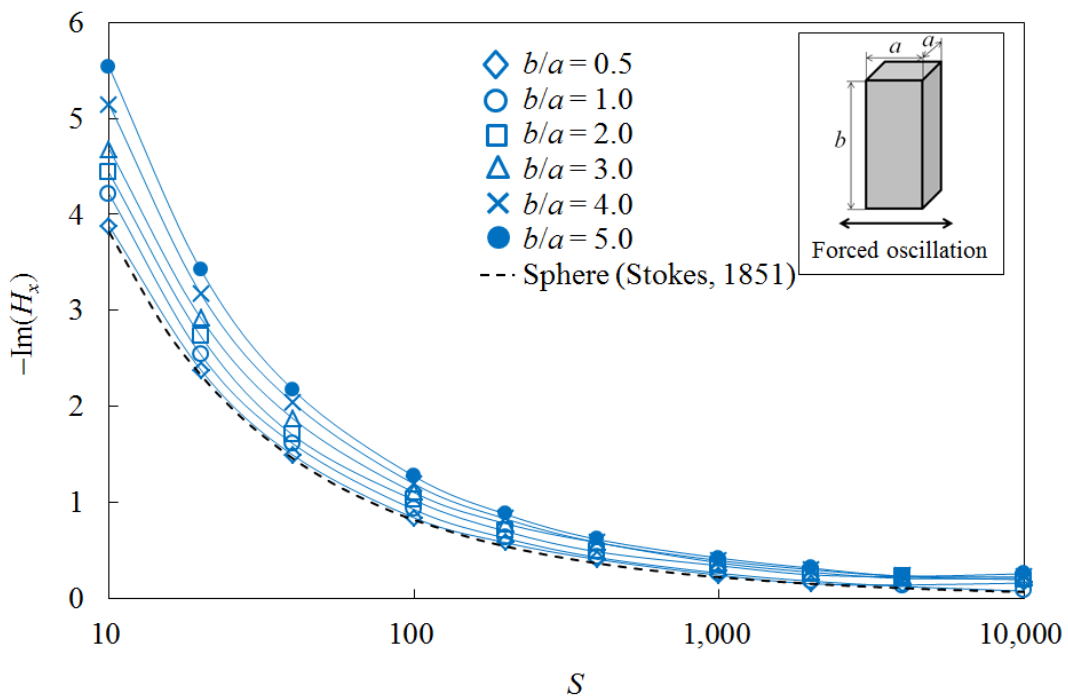
(b) -Im(H_x)

Figure 5: Analytical results of H_x as a function of S
for square-cross-section cylinders with $b/a = 0.5$–5.0 in transverse oscillation.
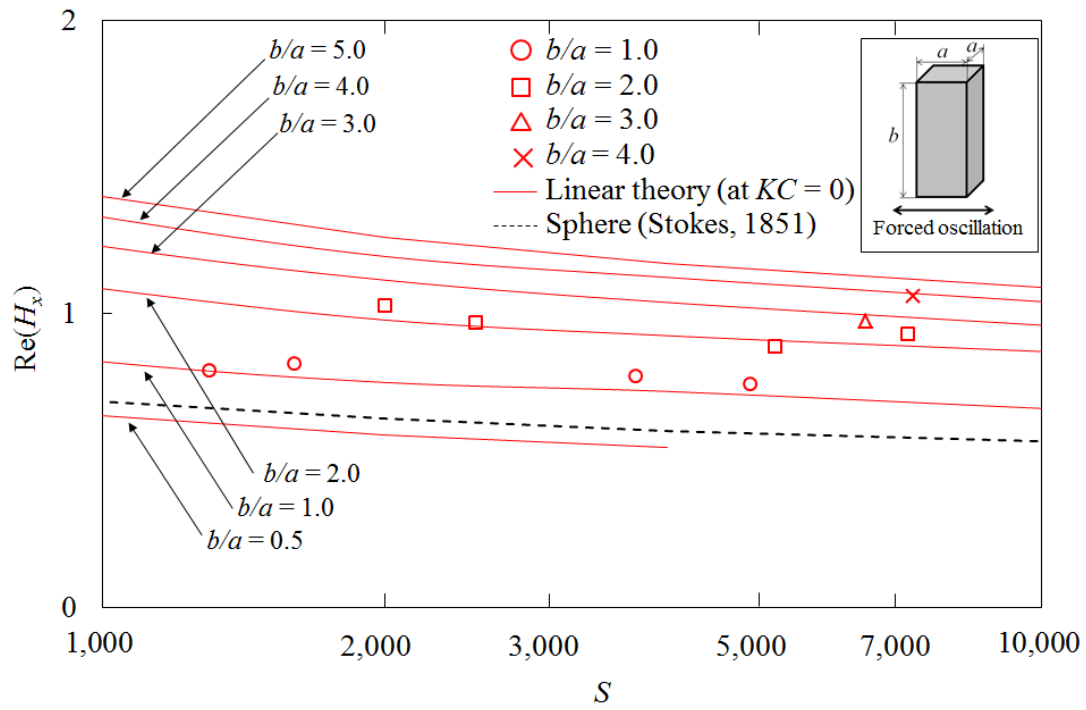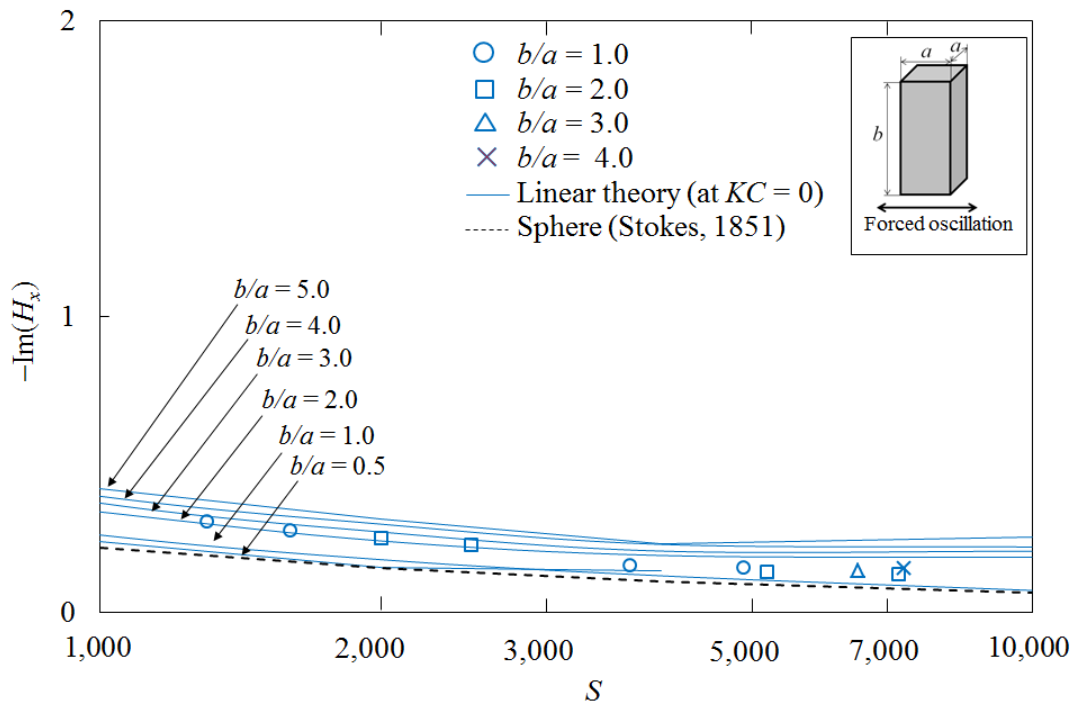
(a) Re(H_x)

(b) -Im(H_x)

Figure 6: Experimental results of H_x at $S = 4,900$ against KC

for a square-cross-section cylinder with $b/a = 1.0$ (a cube) in transverse oscillation.

(a) Re(H_x)

(b) -Im(H_x)

Figure 7: Experimental results of H_x at $KC \cong 0$ as a function of S for square-cross-section cylinders with b/a = 1.0–4.0 in transverse oscillation.